Molecular Imaging
Volume 15: 1-12

DOI: 10.1177/1536012116683597
journals.sagepub.com/home/mix
SAGE

Imaging Bone–Cartilage Interactions in Osteoarthritis Using [^{18}F]-NaF PET-MRI

Dragana Savic, MSc[1,2], Valentina Pedoia, PhD[1], Youngho Seo, PhD[1], Jaewon Yang, PhD[1], Matt Bucknor, MD[1], Benjamin L. Franc, MD[1], and Sharmila Majumdar, PhD[1]

Abstract

Purpose: Simultaneous positron emission tomography–magnetic resonance imaging (PET-MRI) is an emerging technology providing both anatomical and functional images without increasing the scan time. Compared to the traditional PET/computed tomography imaging, it also exposes the patient to significantly less radiation and provides better anatomical images as MRI provides superior soft tissue characterization. Using PET-MRI, we aim to study interactions between cartilage composition and bone function simultaneously, in knee osteoarthritis (OA).

Procedures: In this article, bone turnover and remodeling was studied using [^{18}F]-sodium fluoride (NaF) PET data. Quantitative MR-derived $T_{1\rho}$ relaxation times characterized the biochemical cartilage degeneration. Sixteen participants with early signs of OA of the knee received intravenous injections of [^{18}F]-NaF at the onset of PET-MR image acquisition. Regions of interest were identified, and kinetic analysis of dynamic PET data provided the rate of uptake (K_i) and the normalized uptake (standardized uptake value) of [^{18}F]-NaF in the bone. Morphological MR images and quantitative voxel-based $T_{1\rho}$ maps of cartilage were obtained using an atlas-based registration technique to segment cartilage automatically. Voxel-by-voxel statistical parameter mapping was used to investigate the relationship between bone and cartilage.

Results: Increases in cartilage $T_{1\rho}$, indicating degenerative changes, were associated with increased turnover in the adjoining bone but reduced turnover in the nonadjoining compartments. Associations between pain and increased bone uptake were seen in the absence of morphological lesions in cartilage, but the relationship was reversed in the presence of incident cartilage lesions.

Conclusion: This study shows significant cartilage and bone interactions in OA of the knee joint using simultaneous [^{18}F]-NaF PET-MR, the first in human study. These observations highlight the complex biomechanical and biochemical interactions in the whole knee joint in OA, which potentially could help assess therapeutic targets in treating OA.

Keywords

PET-MRI, multimodality imaging, knee osteoarthritis, sodium fluoride imaging, bone–cartilage interactions, $T_{1\rho}$ relaxation times, voxel-by-voxel statistical parameter mapping, bone remodeling, cartilage degeneration

Introduction

Osteoarthritis (OA) is a degenerative joint disease and a leading cause of chronic disability in the United States. The initial signs of OA include cartilage degeneration manifested as molecular and biochemical changes within the extracellular matrix. Changes in joint kinematics and biomechanical load distribution have been implicated in the initiation of OA. A conservative overall estimate of OA prevalence in the United States was estimated to be 26.9 million US adults in 2005.[1] The incidence of OA is expected to increase to 59 million by the year 2020.[2] The World Health Organization estimates OA to be the leading cause of chronic disability in 10% of the population older than 60 years,[3] and knee OA is associated with chronic disability as often as heart and lung disease.[4]

[1] Department of Radiology and Biomedical Imaging, University of California, San Francisco, San Francisco, CA, USA
[2] Department of Physiology, Anatomy and Genetics, University of Oxford, Oxford, United Kingdom

Submitted: 13/06/2016. Revised: 05/10/2016. Accepted: 14/11/2016.

Corresponding Author:
Dragana Savic, Department of Radiology and Biomedical Imaging, University of California, San Francisco, San Francisco, CA 94143, USA.
Email: dragana.savic@dpag.ox.ac.uk

Joint space narrowing (JSN), as measured by radiographs, is the current gold standard and the criterion for OA progression in clinical trials as accepted by the Food and Drug Administration. Radiograph-based Kellgren-Lawrence (KL)[5] scores are used to categorize participants based on the severity of OA. Long before changes in joint space can be detected, and morphological changes in cartilage occur, a depletion of proteoglycan and an increase in water content and disruption of the collagen network occurs. The symptoms include stiffness, limited joint function, and pain, which lead to a decrease in quality of life. Pain is one of the most important outcome measures in OA and is measured using questionnaires and patient-reported outcomes, such as the Knee Osteoarthritis Outcome Score (KOOS). The early biochemical changes in cartilage are not reflected in the KL grade or JSN from radiographs, but the KOOSs or pain is a measure of symptomatic OA.

Magnetic resonance imaging (MRI), with its superior soft tissue contrast, image resolution, and 3-dimensional (3D) imaging capabilities, has been widely studied in an effort to develop quantitative biomarkers for OA and fill the void that exists for diagnosis, monitoring, and assessment of soft tissue characterization and whole-joint degeneration in OA. Scoring systems such as the Whole-Organ Magnetic Resonance Imaging Score (WORMS)[6] grade cartilage lesions and correlate lesion severity with other findings such as meniscal defects, the presence of bone marrow lesions, as well as radiographic and clinical scores.[7-9] Magnetic resonance-derived $T_{1\rho}$ and T_2 assess the structural and biochemical properties of cartilage such as changes in collagen (T_2)[10] and proteoglycan ($T_{1\rho}$),[11,12] which are both increased in patients with OA compared to control groups.[13,14] In addition to differences in mean and compartmental averages of $T_{1\rho}$ and T_2, studies have demonstrated differences in the spatial heterogeneity of these measures between normal controls and patients with OA.[15-17]

Early changes in OA are also seen in the adjoining subchondral and trabecular bone. Articular cartilage and subchondral bone act in concert during mechanical loading of the joint. The subchondral mineralized zone plays an important role in reducing the axial impact forces, typically encountered during dynamic joint loading[18] and adapts to the mechanical demands during normal and abnormal joint loading.[19-21] A hypothetical model for OA pathogenesis has been proposed by Burr and Gallant,[22] whereby repetitive joint loading causes an initial increase in bone remodeling that is associated with increased vascular invasion of the deep layers of cartilage, which allows unopposed access to the cartilage by chondrolytic enzymes. These enzymes cause a breakdown of the extracellular matrix, loss of proteoglycan and collagen, and thus a loss of cartilage compressive stiffness, and an overload of the joint. Some of these bone remodeling changes are visible on positron emission tomography (PET) imaging. Paradoxically both early-stage increased remodeling and bone loss and the late-stage slow remodeling and subchondral densification are important components of the pathogenic process that leads to OA.

Using MRI for quantifying trabecular architecture, investigators have found a relationship between bone structure and articular cartilage morphology in patients with OA, especially the loss of trabecular bone in regions not adjoining the regions of cartilage loss.[23,24] Subchondral bone changes are present prior and during the development of OA and increased bone blood flow and bone remodeling, as demonstrated by [^{18}F]-sodium fluoride (NaF) PET,[25] may be associated with patellofemoral pain and later stage morphological changes in cartilage. Draper et al[25] showed that pain is correlated to mean normalized standardized uptake value (SUV) measures obtained from PET imaging; so detecting early changes in bone remodeling could help in understanding the disease, relate it to changes in cartilage and whole-joint degeneration and possibly prevent the progression of OA, and provide strategies for reducing symptomatic OA in the future. As the authors[25] describe that even though most edema and cartilage lesions are present, bone metabolic abnormalities are seen where no lesions or structural changes are present on MR images.

The primary goal of this first-in-human study was to demonstrate bone–cartilage interactions in the whole knee joint in patients with OA using simultaneous PET-MRI to understand the pathophysiology of the disease. Positron emission tomography and MR provide different information about the OA in a patient and by combining these two modalities, we can obtain better and more accurate information about the pathophysiology of the disease and its progression.

The interaction between the bone and the cartilage is especially critical in early onset of the disease not only to determine the disease profile but also be able to detect early changes that most likely will show in the bone and therefore will be visible on PET imaging prior to the MRI of the disease.

With simultaneous detection of early cartilage biochemical degeneration using quantitative MR and bone remodeling in adjoining and nonadjoining regions, we can elucidate the natural history of the disease and assess therapeutic targets in the treatment of OA in the future.[26,27]

Materials and Methods

Patient Population

Sixteen patients with knee OA (radiographic or symptomatic) were recruited compliant with the regulations of the Committee of Human Research (CHR), the institutional review board (IRB) at the University of California, San Francisco. Prior to the start of the study, all patients signed a written consent form approved by the CHR. The inclusion criteria were age >35 years, knee pain, aching, or stiffness on most days per month during the past year, or use of medication for knee pain on most days per month during the past year. The exclusion were (1) concurrent use of an investigational drug, (2) history of fracture or surgical intervention in the study knee, and (3) contraindications to MR. Radiographs were obtained from all patients to determine the KL score as a metric of prevalence and severity of radiographic OA. The score ranged from 0 to 4, where 0 showed no features of OA on the radiographs and 4 showed large osteophytes, JSN, severe sclerosis, and definite bony deformity.[5]

All patients filled the validated patient-reported outcomes questionnaire (KOOS)[28] that provided a metric of pain,

Table 1. Magnetic Resonance Imaging Acquisition Parameters.[a]

MR Imaging Sequence	Acquisition Parameters	Measurements
3 plane gradient echo		Localizer – For Choosing Coverage
High resolution 3D FSE (Cube)	TR/TE = 1500/26.69 ms, FOV = 16 cm, Matrix size = 384 x 384, Echo train = 32, Slice thickness = 0.5	Semi-quantitative scores WORMS
Quantitative combined $T_{1\rho}$ /T_2 mapping using MAPSS[b]	TE = 0/12.87/25.69/51.39 ms, TSL = 0/10/40/80 ms, Locking Frequency = 500 Hz, FOV = 14 cm, Matrix size = 256 x 128, Slice thickness = 4.0 mm	Cartilage/Meniscus $T_{1\rho}$ and T_2 mean, laminar

Abbreviations: 3D, three-dimensional; FSE, fast spin echo; MRI, magnetic resonance imaging; TE, echo time; TR, repetition time; WORMS, Whole-Organ Magnetic Resonance Imaging Score; TSL, Spin-Lock Time; FOV, Field of View.
[a]The table lists the MR acquisition parameters for the 3 MR sequences used: (1) localizer, (2) high-resolution 3D FSE CUBE, and (3) quantitative combined $T_{1\rho}/T_2$.
[b]Xiaojan LI, *Magn Reson Med*. In vivo T(1rho) mapping in cartilage using 3D magnetization-prepared angle-modulated partitioned k-space spoiled gradient echo snapshots (3D MAPSS). *Magn Reson Med*. 2008 Feb; 59(2):298-307.

Table 2. Positron Emission Tomography Acquisition Parameters.[a]

Dynamic PET acquisition parameters	
Acquisition time	60 min
Onset after injection	0 min
Number of Phases	3
Number of Frames/Phase	12 frames of 10 s 4 frames of 30 s 14 frames of 4min
Transverse Filter Cutoff	3 mm
Subset	28
Iterations/Axil Filter	4/Standard
Measures	SUV_{max}, SUV_{avg}, Slope K_i

Abbreviations: avg, average; PET, positron emission tomography; max, maximum; SUV, standardized uptake value.
[a]The table lists the PET acquisition parameters for the dynamic PET acquisition.

stiffness, and scores ranged from 0 to 100, where lower scores represented higher pain and symptomatic OA.

Positron Emission Tomography-Magnetic Resonance Imaging Examination Protocol

An intravenous catheter was placed, and the patient was positioned feet-first in a 3-T PET-MR scanner (GE Healthcare, Milwaukee, Wisconsin). An external medium-sized RF flex coil (GE Healthcare) was used due to the significantly lower attenuation effect on the PET signal (ie, low rate of stopping, 511 keV photons) compared to the conventional knee coil. The patients were injected with an average of 340.4 MBq of [^{18}F]-NaF at the onset of the PET-MR scan. A dynamic PET scan was acquired from the time of injection for 60 minutes with MR sequences running concurrently. The MRI sequences acquired simultaneously with the PET acquisition were (1) high-resolution 3D fast spin echo (FSE, CUBE) and (2) quantitative sagittal 3D combined $T_{1\rho}/T_2$ (Table 1).[29] All PET reconstructions were performed using 3D Ordered Subsets Expectation Maximization algorithm with time-of-flight temporal resolution of approximately 400 ps. Magnetic resonance acquisition parameters and PET acquisition parameters are shown in Tables 1 and 2, respectively.

Magnetic Resonance Grading for Assessing Cartilage Lesions and OA Status

A board-certified radiologist (M.B.) graded the morphological MR images (CUBE, Table 1) using WORMS grading.[6] Cartilage lesions were graded as WORMS = 0 (normal thickness), WORMS = 1 (normal thickness, but increased signal intensity), WORMS = 2 (partial thickness focal lesion less than 1 cm at greatest width), WORMS = 2.5 (full thickness focal lesion less than 1 cm at greatest width), WORMS = 3 (multiple areas of partial lesions less than 1 cm at greatest width, or a grade 2 lesion wider than 1 cm, but less than 75% of the region), WORMS = 4 (diffuse partial thickness loss greater than 75% of the region), WORMS = 5 (multiple areas of full thickness lesion greater than 1 cm but less than 75% of the region), and WORMS = 6 (diffuse full thickness loss greater than 75% of the region). The summary of patient characteristics is shown in Table 3.

Positron Emission Tomography Image Analysis

Physiologically, after intravenous injection of the radiopharmaceutical, [^{18}F] ions are extracted from plasma in proportion to bone perfusion and quantitative studies of uptake are possible using dynamic PET.[30] The uptake of the fluoride ion in bone is rapid and the initial uptake is a function of bone blood flow; after residing in the perivascular fluid, an exchange of the fluoride ion with hydroxyl groups in the hydroxyapatite occurs and this is proportional to the surface area of the bone available, which is typically higher in immature bone, with high osteoblastic activity and remodeling.[31,32] The rate constants for these physiological processes calculated by the Patlak analysis method using dynamic multiframe data of PET in a region of interest (ROI) involves linear regression of curve fitting. Hawkins et al showed that a multicompartment nonlinear model including both bound and unbound fluoride ions were in good agreement with Patlak analysis as used in this study.[33] The Patlak graphical analysis method provided the influx rate constant K_i from the slope of the linear portion of the plot, reflecting bone remodeling. Both kinetic and simplified models have been shown to accurately quantify bone turnover using [^{18}F]-NaF PET.[34] The most widely used parameters for semiquantification of PET measures, which do not require dynamic acquisitions, are the standardized uptake values (SUV_{avg} and

Table 3. Patient Evaluation.[a]

Patient	Age, Years	BMI, kg/m^2	NaF, MBq	KL Grade	KOOS Pain	WORMS					
						P	TrF	MF	LF	MT	LT
1	52.00	26.31	329.3	3	100	2	3	3	0	3	1
2	53.00	29.13	340.4	1	100	0	0	0	0	0	0
3	60.00	19.37	340.4	1	83.33	2.5	0	0	0	0	1
4	74.00	26.95	366.3	1	100	3	0	0	0	0	0
5	38.00	24.66	362.6	0	97.22	0	0	0	0	0	0
6	47.00	19.14	284.9	0	44.44	0	0	0	0	0	0
7	57.00	27.02	240.5	1	100	2	2	0	0	0	0
8	64.00	25	358.9	0	91.67	1	0	0	0	0	0
9	54.00	21.12	355.2	3	91.67	3	2.5	0	0	0	0
10	60.00	27.29	340.4	2	61.11	2	0	0	0	0	0
11	40.00	24.33	362.6	0	50	0	0	0	0	0	0
12	59.00	29.41	299.7	0	30.56	0	3	0	0	0	0
13	59.00	18.72	370	0	50	3	0	0	0	0	0
14	66.00	21.42	340.4	0	94.44	0	2	0	0	0	0
15	61.00	31.62	351.5	2	100	4	0	2	2	0	2
16	59.00	28.17	358.9	0	50	2.5	3	0	6	0	6

Abbreviations: BMI, body mass index; KL, Kellgren-Lawrence; KOOS, Knee Osteoarthritis Outcome Score; LF, lateral femur; LT, lateral tibia; MF, medial femur; MT, medial tibia; NaF, sodium fluoride; P, patella; TrF, trochlea; WORMS, Whole-Organ Magnetic Resonance Imaging Score.
[a]Data are for all patients. Age, BMI, and [^{18}F]-NaF injected (MBq) for each patient. KL grade based on radiographs are listed, as well as KOOS pain from the questionnaires and WORMS grades in each cartilage region.

Table 4. Summary of Patient Data.[a]

	P	TrF	MF	LF	MT	LT
PET variables						
Slope K_i avg	0.0048	0.0021	0.0026	0.0026	0.0025	0.0025
Slope K_i std	0.0039	0.0014	0.0015	0.0014	0.0010	0.0012
SUV_{avg} avg	1.4	0.7	0.8	0.8	0.8	0.8
SUV_{avg} std	1.1	0.3	0.4	0.5	0.4	0.3
SUV_{max} avg	3.6	1.5	1.7	1.7	1.7	1.6
SUV_{max} std	2.9	0.8	0.8	0.9	0.7	0.8
Quantitative MR variables						
$T_{1\rho}$ avg	42.6	44.4	41.6	41.2	36.9	34.9
$T_{1\rho}$ std	4.5	4.7	3.6	5.1	4.8	5.8

Abbreviations: avg, average; KL, Kellgren-Lawrence; KOOS, Knee Osteoarthritis Outcome Score; LF, lateral femur; LT, lateral tibia; max, maximum; MF, medial femur; MR, magnetic resonance; MT, medial tibia; P, patella; PET, positron emission tomography; std, standard; TrF, trochlea.
[a]Positron emission tomography and MR variables as well as radiographic scorings (KL) of the patient. The KOOS pain scores grouped from 0 (high pain) to 100 (no pain) and the number of patients (n). Average and standard deviation values are presented for PET and MR variables in all compartments (P, TrF, MF, LF, MT, and LT).

SUV_{max}) that are a measure of uptake and bone remodeling in case of [^{18}F]-NaF, within a ROI decay corrected and normalized for the injected activity and for patient weight or lean body mass.

All bone ROIs were manually segmented as circular regions of interest in PMOD (PMOD Technologies Ltd, Zurich, Switzerland). All bone regions that were segmented were adjacent to the respective cartilage regions (ROIs)—patella (P), trochlea (TrF), medial femur (MF), medial tibia (MT), lateral femur (LF), and lateral tibia (LT). The regions were the same size across all patients and did not overlap with the cartilage. The last 10 minutes of the 60-minute dynamic PET acquisition were summed, and the data were analyzed with both maximum and average SUVs (SUV_{max} and SUV_{avg}). The entire 60-minute PET acquisition was used to do kinetic analysis by using the data from an ROI placed in the popliteal artery as the input function. The input function was corrected for the partial volume effect by acquiring phantom data with different sized cylinders, with known activity and correcting for the partial volume. The 60-minute dynamic PET data were assessed using a linear Patlak graphical analysis method; the slope from the Patlak plot, K_i (ie, [^{18}F]-NaF influx rate contrast—an estimate of uptake rate) in each bone compartment (adjacent to the cartilage compartments) was computed. Average and maximum SUVs (SUV_{avg} and SUV_{max}) and the K_i values can be seen in Table 4.

Quantitative MR Image Analysis

All cartilage regions were automatically segmented as described by Pedoia et al.[35] One patient with average weight and body mass index (BMI) was selected as the reference. Six ROIs were semiautomatically segmented on the reference image—P, TrF, MF, LF, MT, and LT. The 3D FSE CUBE previously rigidly registered on the first Spin-Lock Time (TSL) image of $T_{1\rho}$ sequence was used for the semiautomatic segmentation of the reference. Piecewise rigid registration was applied along the echoes to take into account nonrigid movement of the articulation during the scan. Cartilage ROIs were used to define the borders of the 3 masks that only included the femur, tibia, and P bones. Those masks were then used to constrain the piecewise registration. Each registration was initialized by the results of the one obtained on the previous echo; this approach allowed for good registration performances even in the later echoes characterized by poor SNR.

Nonrigid registration of all images on the reference space was performed. $T_{1\rho}$ maps were obtained by fitting the transformed $T_{1\rho}$-weighted images using a Levenberg-Marquardt monoexponential, ($S(\mathrm{TSL}) \propto e^{-\mathrm{TSL}/T_{1\rho}}$), applied on each voxel. After the registration, the reference's ROIs were overlaid on all maps in the data set allowing for a fully automatic atlas-based segmentation and voxel-based analysis of comparative regions between patients. This allowed for analyzing data-driven subcompartments and layers based in the relaxation parameters pattern instead of defining a priori subdivision. Pearson partial correlation was used to assess association between bone remodeling and cartilage biochemistry measures at the voxel-level adjusting for age, gender, BMI, and KOOS pain. An R value volumetric statistical parametric maps (SPMs) for each measure was obtained in the overall segmented cartilage. Clusters of significant voxels were defined with the same R sign and $P < .05$. Significance could be viewed at the level of the individual voxels; however, to avoid by chance correlations, a size threshold was set such that a cluster of adjacent neighboring pixels was considered for further analysis, if the size of the cluster (number of voxels in the cluster) relative to the total number of voxels in the compartment was greater than or equal to 8% of the size of the entire compartment. This threshold was selected empirically and kept constant.

Three-dimensional representations of the SPM were generated using a technique based on Laplace equation, previously used to generate cartilage thickness maps.[36] The technique yields a one-to-one matching between points in the bone–cartilage interface and points in the articular surface with no crossings. Laplace equation was numerically solved in 3 dimensions with Dirichlet boundary conditions obtaining a potential map. A vector field was generated to lead each point in the bone–cartilage interface to a point in the articular surface. Average R values along this trajectory are computed and projected on the triangulated mash obtained from 3D bone segmentation of the reference knee. A visual inspection of the SPMs was then conducted to identify global pattern of association between bone remodeling and cartilage relaxation times.

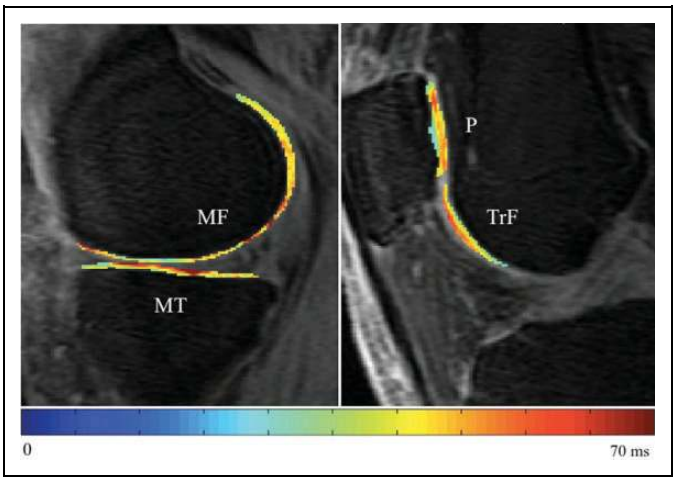

Figure 1. Voxel-based $T_{1\rho}$ maps. An atlas-based voxel-by-voxel $T_{1\rho}$ map that shows regions in the medial tibia (MT), the medial femur (MF), patella (P), and in the trochlea (TrF). The $T_{1\rho}$ color maps are overlaid on a gray scale magnetic resonance (MR) image and the color bar represents relaxation times from 0 ms (blue) to 70 ms (red).

Results

Study Population

Sixteen patients with varying degrees of knee OA were studied using an integrated PET-MR system (GE Healthcare, Waukesha, Wisconsin). Table 3 lists the patient demographics, isotope dose, the OA status, and pain. The average age of the patients was 57 years and average BMI was 25.3 kg/m^2. The average [^{18}F]-NaF dose injected was 340.4 MBq in 11 males and 5 females. Twelve of the patients had minimal or no sign of radiographic OA (KL grade 0 and 1); however, they did have some pain based on the KOOS questionnaires. Four of the patients had either KL grade 2 (definite osteophytes—possible JSN) or KL grade 3 (multiple osteophytes—definite JSN—possible bony deformity). The patients had varying degrees of pain assessed using the patient-reported questionnaire—KOOS (average KOOS = 78; range, 30.6-100). Magnetic resonance-derived WORMSs showed the highest lesion load in the patellar cartilage (Table 3). Quantitative MR images provided $T_{1\rho}$ in each of the above cartilage compartments (Table 4). Figure 1 shows an example of the $T_{1\rho}$ map of a patient with KL grade 2 and WORMS grade 2 in the TrF. In this example, the high spatial heterogeneity of the cartilage composition is notable; clusters of higher $T_{1\rho}$ in the articular layer of the P and the TrF as well as in the MT are demonstrated.

Quantitative and Semiquantitative PET

The average and maximum [^{18}F]-NaF uptake values as $\mathrm{SUV_{avg}}$ and $\mathrm{SUV_{max}}$ in all bone compartments (Figure 2A) were plotted against [^{18}F]-NaF uptake rate (slope K_i), which is obtained from kinetic modeling with a linear Patlak method. Slope K_i correlate with the semiquantitative $\mathrm{SUV_{avg}}$ and $\mathrm{SUV_{max}}$ ($R^2 = .7$) in all bone compartments (Figure 2B and C).

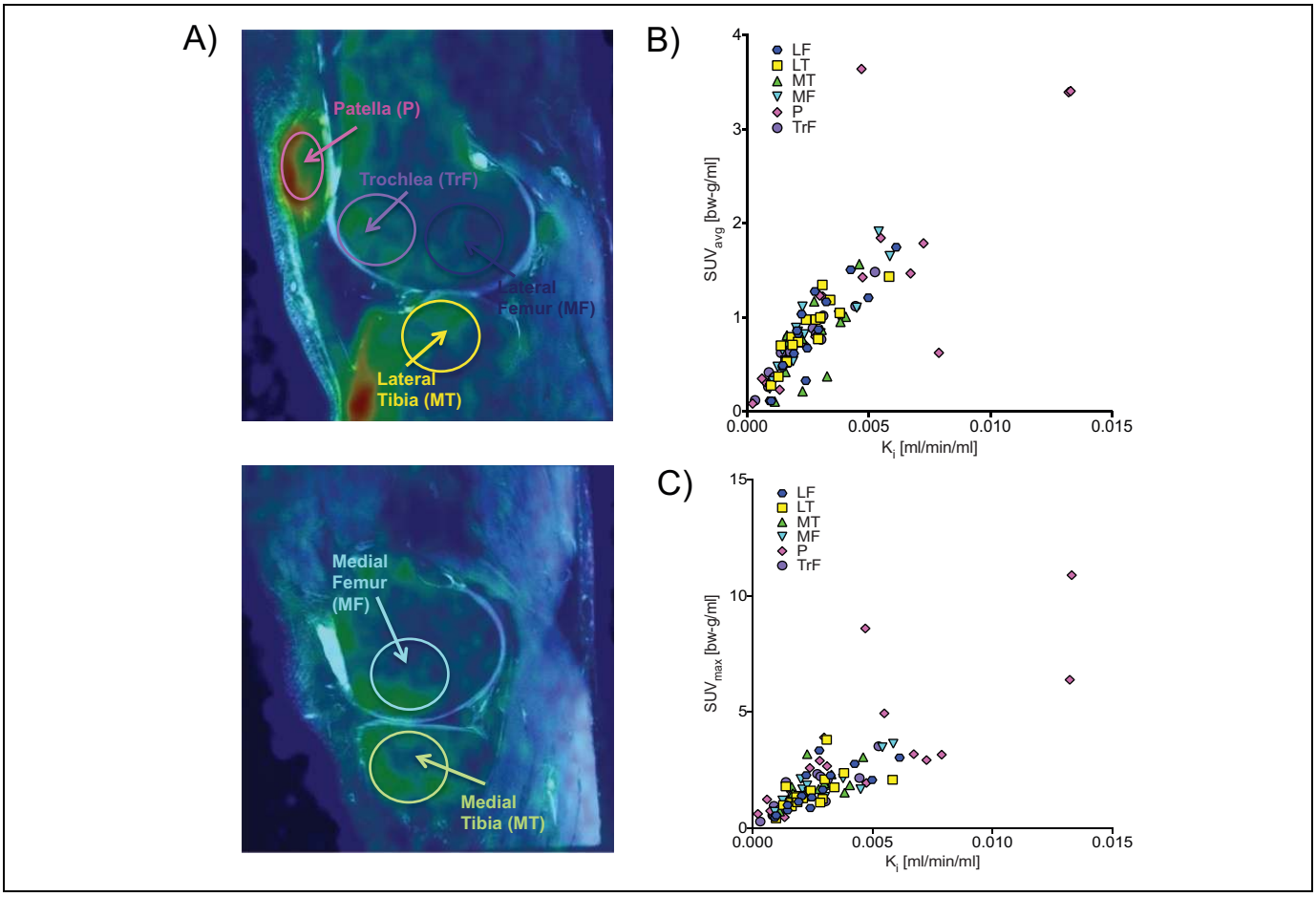

Figure 2. Correlations between quantitative and semiquantitative positron emission tomography (PET) measures. A, PET-magnetic resonance (MR) fused image in the lateral and medial side of the knee. Bone compartments are showed as regions of interest (ROIs) in the lateral and medial side of the knee in compartments—patella (P), trochlea (TrF), lateral femur (LF), lateral tibia (LT), medial femur (MF), medial tibia (MT). B and C, Correlations between NaF uptake at 60 minutes (standardized uptake value [SUV]) in all bone compartments plotted with the uptake rate (K_i) in the same compartments. SUV_{avg} and SUV_{max} have high correlations with slope K_i ($R^2 = .71$ and 0.69).

The uptake rate defined by slope K_i obtained from the Patlak method in all compartments is presented as (average $\pm$ standard deviation)—P: 0.005 $\pm$ 0.0039, TrF: 0.0023 $\pm$ 0.0017, MF: 0.0028 $\pm$ 0.0017, MT: 0.0028 $\pm$ 0.0014, LF: 0.0028 $\pm$ 0.0015, and LT: 0.0027 $\pm$ 0.0013 (Table 5).

A significant difference (paired t test, $P < .05$) was found in the P compartment compared to all other bone compartments and between the TrF and the LF as well as between the TrF and the MF bone. Ten (63%) patients had the fastest uptake rate in the P (slope K_i). In 25% of the patients, the highest uptake rate was in the lateral and MT resulting in the tibia being the compartment with the second fastest average uptake rate. However, the average slope K_i in the tibia was only significantly different from P (Table 5). The same trends are seen for SUV_{max}, where 63% of the patients have the highest uptake in the P (SUV_{max}) and the second highest [^{18}F]-NaF uptake is found in the femur.

The average standardized uptake values (SUV_{avg}) showed a dependence on the presence of lesions in the P but also on the patient's pain (Table 5). In patients with WORMS of 0 and 1 indicating no lesions, or mild OA, the patients with pain had higher SUV_{avg} values ($SUV_{avg} = 2.0$) compared to those without pain ($SUV_{avg} = 0.9$), showing significant trends, $P < .1$. However, in the presence of morphological lesions in cartilage, WORMS >1, those without pain ($SUV_{avg} = 1.9$) had higher SUV_{avg} values compared to those with pain ($SUV_{avg} = 0.8$), also approaching significance, $P < .1$.

Knee Bone–Cartilage Interactions

Correlations between the remodeling in the bone and degeneration in the cartilage were observed across several bone and cartilage compartments, and interactions were seen in adjacent regions but also in compartments, which were not adjoining. The highest correlations between the PET values from the bone and the $T_{1\rho}$ values from the cartilage were seen with K_i in the MT (Figure 3), and with the SUV_{max} in the P (Figure 4) and in the LT (Figure 5). The color bar ranges from strong negative correlations (light blue, purple, and blue) to strong positive correlations (red, green, and yellow) denoted with a correlation coefficient, R (range: -1.0 to 1.0, where the P value = 0.0001

Table 5. Sodium Fluoride Uptake Associated With Pain.[a]

Kinetic uptake rate of NaF; slope K_i (mean $\pm$ SD)	
P	0.005 ± 0.0040
TrF	0.002 ± 0.0017[b]
LT	0.003 ± 0.0014[b]
MT	0.003 ± 0.0015[b]
LF	0.003 ± 0.0016[b,c]
MF	0.003 ± 0.0017[b,c]
NaF uptake in the P; SUV_{avg} (mean $\pm$ SD)	
No pain, no lesions (WORMS = 0,1)	0.88 ± 0.66[d]
Pain, no lesions (WORMS = 0, 1)	2.03 ± 1.23[d]
No pain, lesions (WORMS > 1)	1.96 ± 1.38[d]
Pain, lesions (WORMS > 1)	0.84 ± 0.81[d]

Abbreviations: KOOS, Knee Osteoarthritis Outcome Score; LF, lateral femur; LT, lateral tibia; MF, medial femur; MT, medial tibia; NaF, sodium fluoride; P, patella; SD, standard deviation; SUV, standardized uptake value; TrF, trochlea; WORMS, Whole-Organ Magnetic Resonance Imaging Score.

[a][^{18}F]-NaF uptake rate (slope K_i) in the bone compartments (mean $\pm$ SD), comparison between compartmental uptake rate found with paired *t* test ($P < .05$). [^{18}F]-NaF uptake (SUV_{avg}) in the bone of the P is divided into those with lesion based on WORMS, and those without lesions, as well if they were with pain (KOOS < 90) or without pain (KOOS > 90), these groups (NaF uptake in the P; SUV_{avg}) were approaching significance with an unpaired *t* test with $P < .1$.

[b]Significance <.05 compared to P.

[c]Significance <.05 compared to TrF.

[d]Approaching significance $P < .1$.

for $R = \pm .8$). A scatterplot for the average values for all patients are depicted in the white box selected regions (Figures 3–5), where there are large clusters of voxels with moderate to strong correlations. The ellipse represents 95% confidence interval.

The slope K_i obtained from the MT bone was correlated with the $T_{1\rho}$ relaxation times in the cartilage of the MT, the posterior MT, P, and TrF (Figure 3).

A strong positive correlation was observed between $T_{1\rho}$ relaxation times in the cartilage of the MT with the MT slope K_i ($R = .68$, $P = .0014$), and similarly in the P ($R = .75$, $P = .0045$), whereas a moderate negative correlation was observed in the TrF with the MT slope K_i ($R = -.48$, $P = .066$; Figure 3).

The SUV_{max} in the P bone was correlated with the $T_{1\rho}$ in the bone layer of the cartilage ($R = .42$, $P = .10$), and the articular layer ($R = .50$, $P = .048$) of the P cartilage, and the SUV_{max} in the P bone was strongly negatively correlated with $T_{1\rho}$ from the TrF cartilage ($R = -.72$, $P = .002$; Figure 4).

The SUV_{max} in the LT bone was correlated with $T_{1\rho}$ in the LT cartilage ($R = .74$, $P = .0042$), LF cartilage ($R = .71$, $P = .0062$), and MF cartilage ($R = -.61$, $P = .012$; Figure 5).

Discussion

Kinetic [^{18}F]-NaF/$T_{1\rho}$ PET-MR studies were performed in patients with different degrees of knee OA at the University of California, San Francisco, to investigate the interaction of the cartilage with the bone. A direct correlation was identified between the cartilage biochemistry, quantitative MR biometrics, and PET evidence of bone remodeling in patients with knee OA. This demonstration of bone–cartilage interactions in patients with knee OA in adjoining and nonadjoining regions leads us to speculate about the concept of the Bone–Cartilage Connectome. Our results support the complex interplay between biomechanics and joint loading as well as biochemistry and tissue degeneration as a composite in OA, a disease affecting the whole joint, showing even trends with pain. Both imaging modalities are critical to obtain a comprehensive overview of the disease to get to the core of the pathophysiology of OA with the aim of treatment; however, larger longitudinal studies are further needed.

Despite the relatively small sample size, the correlations between [^{18}F]-NaF uptake in the bone, morphological lesions in MR, and pain scores approached statistical significance ($P < .1$). Based on our results, we speculate that early OA is initiated by increases in repetitive loading of the P, with subsequent increases in bone remodeling and release of degradative proteinases, which depletes proteoglycan from the extracellular cartilage matrix. On MRI, this manifests as increases in $T_{1\rho}$. Several knee nerve endings are close to the patellar fat pad; we speculate that the degradative enzymes irritate the nerve endings, giving rise to pain. Pain was present in both knees with high and low metabolic activity, with different stages of OA suggesting that pain is complex and subjective. It is likely that the threshold for feeling the pain is dependent on the patient and on the length of the OA disease. Studies showed that pain correlates with T_2 relaxation times in early OA and can therefore be a quantitatively measurable biomarker for knee pain[37,38]; however, due to the small sample size, this only approaches statistical significance in this study. Given these findings, future studies will be able to study pain more thoroughly using the PET-MRI technology and our experimental setup as a basis.

A discrepancy between [^{18}F]-NaF uptake and morphological MR lesions in adjoining regions, along with increased uptake in patients with pain was also seen by Draper et al,[25] using PET/CT and MR that were done sequentially. Our study confirmed the trend, however, our investigation of early changes in cartilage biochemistry, the automatic atlas-based segmentations[35] and voxel-based $T_{1\rho}$, and SPM further revealed complex interactions. Subchondral bone is known to be involved in OA development and subchondral sclerosis is frequently seen in patients with OA, as is trabecular bone osteopenia. It remains unclear whether bone changes precede cartilage deterioration or are involved in the progression of the disease.[39] Interestingly, in this study, in the presence of morphological lesions, lower remodeling was seen in patients with pain. The MR morphological grading demonstrated multiple areas of partial cartilage loss/defect in the TrF but no lesions in the P. Patella showed both the highest and fastest remodeling (Table 5), indicating that loading affects different knee compartments differently, perhaps due to biomechanical loading and perhaps consistent with the findings of Hunter et al who found that knee pain was highly associated to degeneration in the cartilage of the P.[38]

Increased rate of bone turnover using both kinetic and SUV data was seen in several compartments, where uptake of

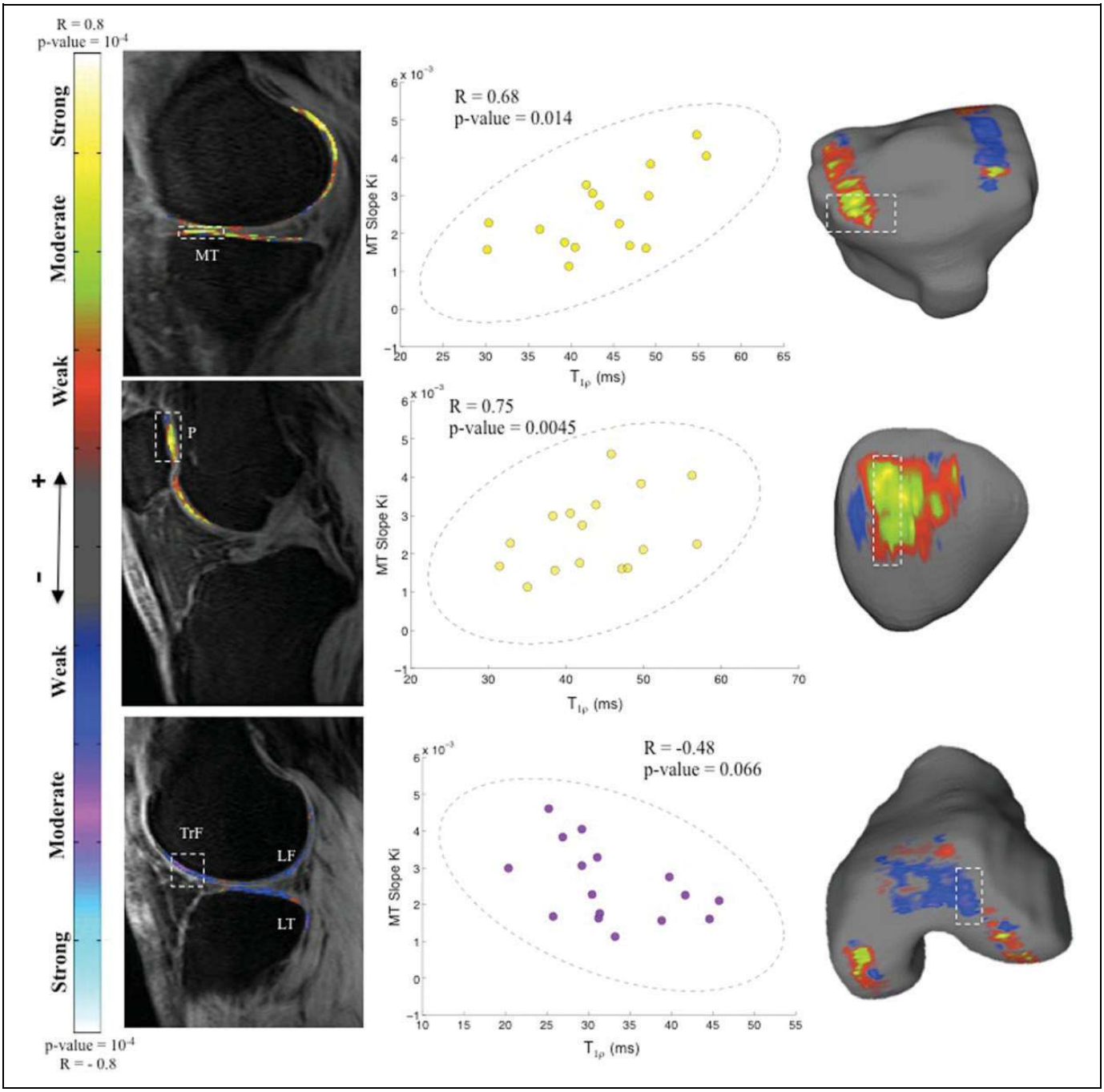

Figure 3. Voxel-based $T_{1\rho}$ maps from the cartilage correlated with slope K_i from the bone of the medial tibia (MT). The color map represents the Pearson correlation *R* values representing positive and negative correlations. The right side shows the scatterplots of the average value of the voxels in white dashed boxes from the magnetic resonance (MR) images. The ellipse illustrates the 95% confidence interval. (Top) Anterior MT cartilage shows a strong positive correlation with the slope K_i from MT bone ($R = .68$, $P = .0014$). (Middle) The patella cartilage shows a strong positive correlation with slope K_i from MT bone ($R = .75$, $P = .0045$). (Bottom) The trochlea (TrF) cartilage shows a moderate negative correlation with slope K_i from MT bone ($R = -.48$, $P = .066$).

[^{18}F]-NaF was seen simultaneously with early degenerative changes in the cartilage. Increased bone turnover was also seen, when there was mechanical overload, such as the contact areas, which can also cause damage to the bone that leads to remodeling, that does not necessary increase the bone density but could cause bone turnover to increase.[40] Burr and Schaffler suggested that it was only the cartilage and the adjacent bone that was significant for the disease progression of OA.[39] However, in this study, we found compelling evidence that it was not only the adjacent regions that affect the health of the knee but also bone remodeling at a greater distance to the cartilage regions with increased stress as seen from $T_{1\rho}$ values from the

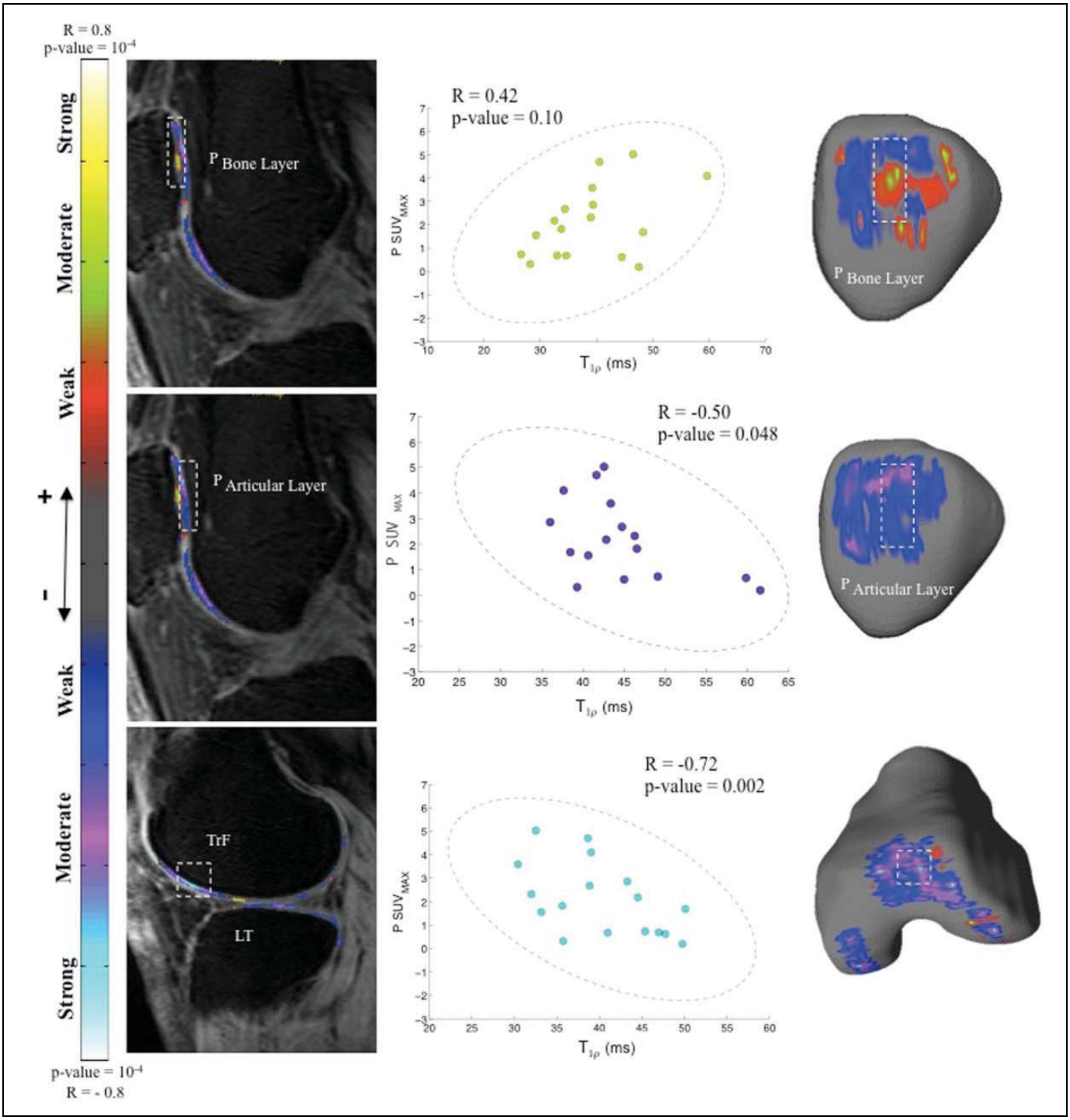

Figure 4. Voxel-based $T_{1\rho}$ maps from the cartilage correlated with standardized uptake value (SUV_{max}) in the bone of the patella (P). The color map represents the Pearson correlation *R* values representing positive and negative correlations. The right side shows the scatterplots of the average value of the voxels in white dashed boxes from the magnetic resonance (MR) images. The ellipse illustrates the 95% confidence interval. (Top) The bone layer of the P cartilage shows a moderate positive correlation with SUV_{max} from the P bone ($R = .42$, $P = .10$). (Middle) The articular layer of the P cartilage shows a moderate negative correlation with SUV_{max} from the P bone ($R = -.50$, $P = .048$). (Bottom) The trochlea (TrF) cartilage shows a strong negative correlation with SUV_{max} from the P bone ($R = -0.72$, $P = .002$).

cartilage. In order to establish the relationship more conclusively, clearly, longitudinal data and larger sample sizes are necessary.

As an example for the nonadjacent connection, the slope K_i from the MT was positively correlated with the $T_{1\rho}$ in the cartilage on the medial femoral-tibia side and on the P and was

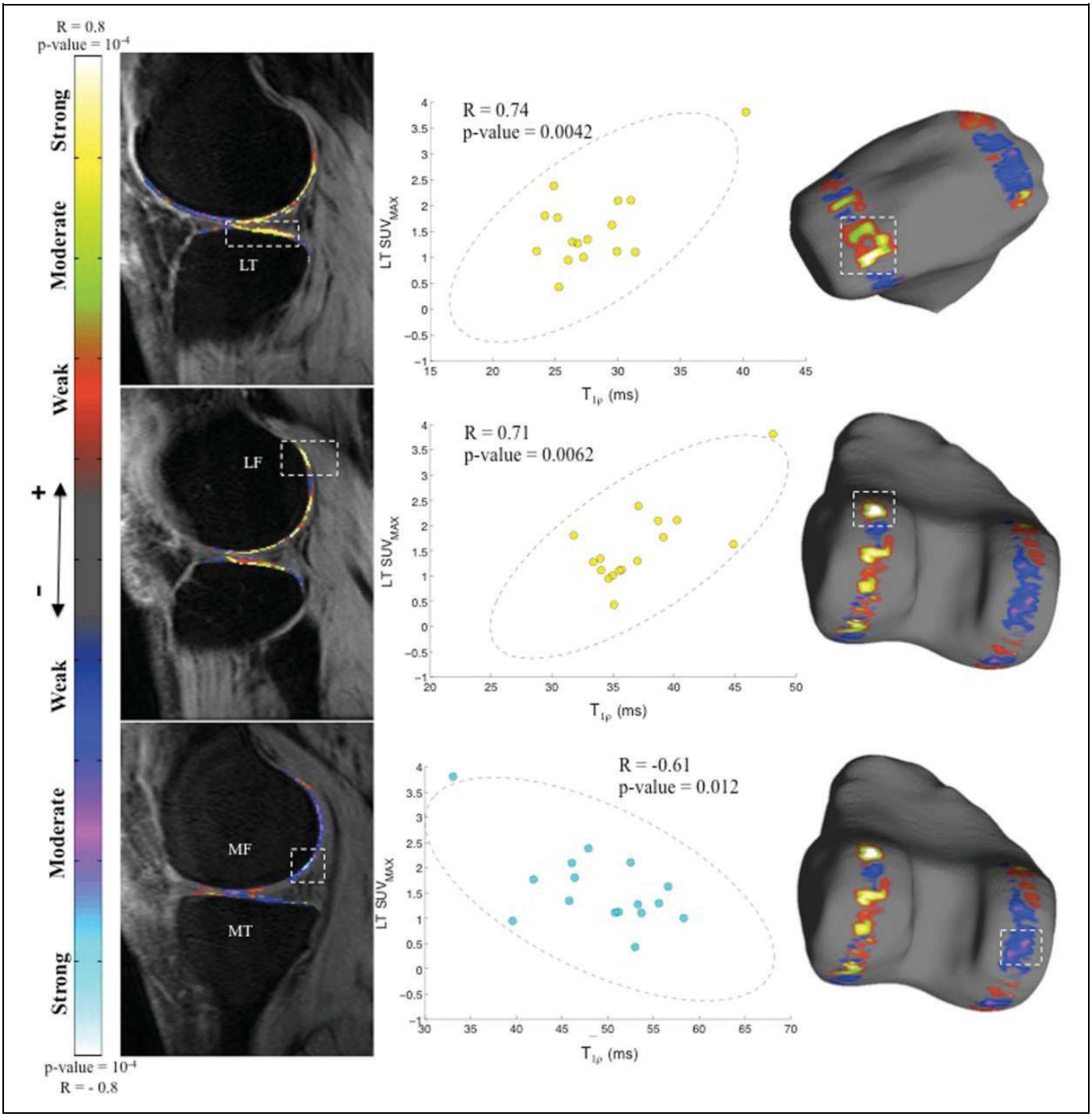

Figure 5. Voxel-based $T_{1\rho}$ maps from the cartilage correlated with standardized uptake value (SUV_{max}) from lateral tibia (LT) bone. The color map represents the Pearson correlation *R* values representing positive and negative correlations. The right side shows the scatterplots of the average value of the voxels in white dashed boxes from the magnetic resonance (MR) images. The ellipse illustrates the 95% confidence interval. (Top) The cartilage of the lateral tibia (LT) shows a strong positive correlation with SUV_{max} from the LT bone ($R = .74$, $P = .0042$). (Middle) The cartilage in the posterior lateral femur shows a strong positive correlation with SUV_{max} from the LT bone ($R = .71$, $P = .0062$). (Bottom) The cartilage in the medial femur (MF) shows a strong negative correlation with SUV_{max} from the LT bone($R = -.61$, $P = .012$).

negatively correlated with $T_{1\rho}$ in the cartilage on the lateral femoral-tibia side of the knee; this could relate to the loading pattern of the knee, so that the loading shifts from the lateral side of the knee to the medial. Vincent et al[41] showed that once OA has occurred, the mechanical and morphological characteristics lead to further degeneration of the cartilage. Using voxel-based relaxometry, we were able to distinguish between different relationships between bone–cartilage associated with the different layers of the cartilage, this was seen in several compartments, such as the TrF and the LT but

especially in the P, that was clearly separated into an articular layer and a bone layer. $T_{1\rho}$ in the 2 layers was differently correlated with the slope K_i of the bone. As a result, we recommend that the cartilage not be treated as a single region, since several significant clusters were observed locally in the different cartilage compartments (Figures 3–5). Our method was more sensitive to local changes in the cartilage and therefore early cartilage degeneration together with bone remodeling might provide us with biomarkers for early OA, changes in which may potentially be reversible.

Although the cartilage and bone has been investigated in patients with knee OA, it has never been assessed simultaneously using the voxel-by-voxel-based concept, relating adjoining and distance regions, and focusing on cartilage biochemical degeneration and bone remodeling as early markers of OA. One of the limitations in this study was the relatively small sample size and the broad range of disease severity. However, the results can be used for hypothesis generation for further elucidating the interaction between bone–cartilage, and clearly further studies are warranted, for example in patients with Anterior Cruciate Ligament (ACL) injury who are at risk of getting OA maybe considered to be a good model for studying early OA changes.[42,43]

Not only have we shown that increased uptake of [^{18}F]-NaF in the knee OA, but we have also shown that quantitative PET metrics correlate with the semiquantitative ($R^2 = .7$) metrics consistent with the literature,[34] thus supporting the use of both metrics to characterize bone remodeling. The benefit of the PET-MR scanner is that it saves time and provides a platform to study direct correlations between cartilage degeneration and the dynamic process of bone remodeling providing a better diagnostic tool for the evaluation of OA. If the kinetic PET data in patients with OA are replaceable by the static data, one can save time on the PET imaging and only acquire short sequences, leaving enough time for example to acquire MR of both knees instead of one. The PET-MR technology together with the initial finding of the connection between the bone and the cartilage can help us understand the disease more thoroughly. However, further studies are needed to evaluate these connections.

The development of effective disease-modifying drugs in OA is in progress to define the molecular mechanisms involved in the initiation and progression of OA. The dysregulation in cartilage breakdown and subchondral bone remodeling may be improved by selective inhibitors of matrix metalloproteinases and proteases.[44] Irrespective of what the molecular target might be, if subchondral bone is targeted, or bone–cartilage interactions are to be considered, it will be important to assess these tissue changes in 3 dimensions across the whole joint.

The interactions between the bone and the cartilage highlight the role of biomechanical loading and thus demonstrates linkages between different regions of the entire knee with regard to the early degenerative changes in cartilage, bone remodeling, and lesion formation can be used to not just diagnose but to also monitor and potentially develop therapeutic approaches at an early stage in order to prevent severe OA.

Acknowledgments

The authors like to thank Melissa Guan, Vahid Ravanfar, Dan Vigneron, Anand Venkatachari, Jim Slater, and Nathan Jenkins for their help with this study and for the endless discussions that contributed to this work. The authors acknowledge the funding sources and research grants from GE Healthcare and from National Institutes of Health P50 AR060752.

Declaration of Conflicting Interests

The author(s) declared no potential conflicts of interest with respect to the research, authorship, and/or publication of this article.

Funding

The author(s) disclosed receipt of the following financial support for the research, authorship, and/or publication of this article: This study was funded by GE Healthcare and research grants from National Institutes of Health P50 AR060752.

References

1. Lawrence RC, Felson DT, Helmick CG, et al; National Arthritis Data Workgroup. Estimates of the prevalence of arthritis and other rheumatic conditions in the United States. Part II. *Arthritis Rheum*. 2008;58(1):26–35.
2. Lawrence RC, Helmick CG, Arnett FC, et al. Estimates of the prevalence of arthritis and selected musculoskeletal disorders in the United States. *Arthritis Rheum*. 1998;41(5):778–799.
3. World Health Organization. *Global Economic and Healthcare Burden of Musculoskeletal Disease*. 2003. http://www.who.int/bulletin/volumes/81/9/Woolf.pdf.
4. Guccione AA, Felson DT, Anderson JJ, et al. The effects of specific medical conditions on the functional limitations of elders in the Framingham Study. *Am J Public Health*. 1994;84(3):351–358.
5. Kellgren J, Lawrence J. Radiologic assessment of osteoarthritis. *Ann Rheum Dis*. 1957;16(4):494–502.
6. Peterfy CG, Guermazi A, Zaim S, et al. Whole-Organ Magnetic Resonance Imaging Score (WORMS) of the knee in osteoarthritis. *Osteoarthritis Cartilage*. 2004;12(3):177–190.
7. Link TM, Steinbach LS, Ghosh S, et al. Osteoarthritis: MR imaging findings in different stages of disease and correlation with clinical findings. *Radiology*. 2003;226(2):373–381.
8. Felson DT, McLaughlin S, Goggins J, et al. Bone marrow edema and its relation to progression of knee osteoarthritis. *Ann Intern Med*. 2003;139(5 pt 1):330–336.
9. Felson DT, Chaisson CE, Hill CL, et al. The association of bone marrow lesions with pain in knee osteoarthritis. *Ann Intern Med*. 2003;134(7):541–549.
10. David-Vaudey E, Ghosh S, Ries M, Majumdar S. T2 relaxation time measurements in osteoarthritis. *Magn Reson Imaging*. 2004;22(5):673–682.
11. Akella SV, Regatte RR, Gougoutas AJ, et al. Proteoglycan-induced changes in T1rho-relaxation of articular cartilage at 4T. *Magn Reson Med*. 2001;46(3):419–423.
12. Wheaton AJ, Casey FL, Gougoutas AJ, et al. Correlation of T1rho with fixed charge density in cartilage. *J Magn Reson Imaging*. 2004;20(3):519–525.

13. Regatte RR, Akella SV, Borthakur A, Kneeland JB, Reddy R. In vivo proton MR three-dimensional T1rho mapping of human articular cartilage: initial experience. *Radiology*. 2003;229(1): 269–274.
14. Li X, Benjamin Ma C, Link TM, et al. In vivo T(1rho) and T(2) mapping of articular cartilage in osteoarthritis of the knee using 3 T MRI. *Osteoarthritis Cartilage*. 2007;15(7):789–797.
15. Carballido-Gamio J, Link TM, Majumdar S. New techniques for cartilage magnetic resonance imaging relaxation time analysis: texture analysis of flattened cartilage and localized intra- and inter-subject comparisons. *Magn Reson Med*. 2008;59(6):1472–1477.
16. Carballido-Gamio J, Stahl R, Blumenkrantz G, Romero A, Majumdar S, Link TM. Spatial analysis of magnetic resonance T1rho and T2 relaxation times improves classification between subjects with and without osteoarthritis. *Med Phys*. 2009;36(9): 4059–4067.
17. Schooler J, Kumar D, Nardo L, et al. Longitudinal evaluation of T1rho and T2 spatial distribution in osteoarthritic and healthy medial knee cartilage. *Osteoarthritis Cartilage*. 2014;22(1): 51–62.
18. Radin E, Rose R. Role of subchondral bone in the initiation and progression of cartilage damage. *Cin Orthop Relat Res*. 1986; (213):34–40.
19. Muller-Gerbl M, Griebl R, Putz R, Golman A, Kuhr M, Taeger K. Assessment of subchondral bone density distribution patterns in patients subject to correction osteotomy. *Trans Orth Soc*. 1994; 19:574.
20. Muller-Gerbl M, Putz R, Hodapp N, Schulte E, Wimmer B. Computer tomography osteo-absorptiometry for assessing the density distribution of subchondral bone as a measure of long term mechanical adaptation in individual joints. *Skeletal Radiol*. 1989;18(7):507–512.
21. Pauwels F. *Biomechanics of the Locomotor Apparatus*. Berlin, Germany: Springer; 1980.
22. Burr DB, Gallant MA. Bone remodelling in osteoarthritis. *Nat Rev Rheumatol*. 2012;8(11):665–673.
23. Lindsey CT, Narasimhan A, Adolfo JM, et al. Magnetic resonance evaluation of the interrelationship between articular cartilage and trabecular bone of the osteoarthritic knee. *Osteoarthritis Cartilage*. 2004;12(2):86–96.
24. Bolbos RI, Zuo J, Banerjee S, et al. Relationship between trabecular bone structure and articular cartilage morphology and relaxation times in early OA of the knee joint using parallel MRI at 3 T. *Osteoarthritis Cartilage*. 2008;16(10):1150–1159.
25. Draper CE, Quon A, Fredericson M, et al. Comparison of MRI and (1)(8)F-NaF PET/CT in patients with patellofemoral pain. *J Magn Reson Imaging*. 2012;36(4):928–932.
26. Karsdal MA, Leeming DJ, Dam EB, et al. Should subchondral bone turnover be targeted when treating osteoarthritis? *Osteoarthritis Cartilage*. 2008;16(6):638–646.
27. Karsdal MA, Sondergaard BC, Arnold M, Christiansen C. Calcitonin affects both bone and cartilage: a dual action treatment for osteoarthritis? *Ann N Y Acad Sci*. 2007;1117:181–195.
28. Roos EM, Lohmander LS. The Knee injury and Osteoarthritis Outcome Score (KOOS): from joint injury to osteoarthritis. *Health Qual Life Outcomes*. 2003;1:64.
29. Li X, Wyatt C, Rivoire J, et al. Simultaneous acquisition of T1γ and T2 quantification in knee cartilage: repeatability and diurnal variation. *J Magn Reson Imaging*. 2014;39(5):1287–1293.
30. Nahmias C, Cockshott WP, Belbeck LW, Garnett ES. Measurement of absolute bone blood flow by positron emission tomography. *Skeletal Radiol*. 1986;15(3):198–200.
31. Blau M, Ganatra R, Bender MA. 18F-fluoride for bone imaging. *Semin Nucl Med*. 1972;2(1):31–37.
32. Irmler IM, Gebhardt P, Hoffmann B, et al. 18 F-Fluoride positron emission tomography/computed tomography for noninvasive in vivo quantification of pathophysiological bone metabolism in experimental murine arthritis. *Arthritis Res Ther*. 2014;16(4): R155.
33. Hawkins RA, Choi Y, Huang SC, et al. Evaluation of skeletal kinetics of fluorine 18-fluoride ion with PET. *J Nucl Med*. 1991;33(5):633–642.
34. Raijmakers P, Temmerman OP, Saridin CP, et al. Quantification of 18F-fluoride kinetics: evaluation of simplified methods. *J Nucl Med*. 2014;55(7):1122–1127.
35. Pedoia V, Li X, Su F, Calixto N, Majumdar S. Fully automatic analysis of the knee articular cartilage T relaxation time using voxel-based relaxometry. *J Magn Reson Imaging*. 2016;43(4): 970–980.
36. Carballido-Gamio J, Majumdar S. Atlas-based knee cartilage assessment. *Magn Reson Med*. 2011;66(2):574–583.
37. Baum T, Joseph GB, Arulanandan A, et al. Association of magnetic resonance imaging-based knee cartilage T2 measurements and focal knee lesions with knee pain: data from the osteoarthritis initiative. *Arthritis care res (Hoboken)*. 2012; 64(2):248–255.
38. Hunter DJ, March L, Sambrook PN. The association of cartilage volume with knee pain. *Osteoarthritis Cartilage*. 2003;11(10): 725–729.
39. Burr DB, Schaffler MB. The involvement of subchondral mineralized tissues in osteoarthrosis: quantitative microscopic evidence. *Microsc Res Tech*. 1997;37(4):343–357.
40. Burr DB. The importance of subchondral bone in the progression of osteoarthritis. *J Rheumatol Suppl*. 2004;70:77–80.
41. Vincent KR, Conrad BP, Fregly BJ, Vincent HK. The pathophysiology of osteoarthritis: a mechanical perspective on the knee joint. *PM R*. 2012;4(5 suppl):S3–S9.
42. Zaid M, Lansdown D, Su F, et al. Abnormal tibial position is correlated to early degenerative changes one year following ACL reconstruction. *J Orthop Res*. 2015;33(7):1079–1086.
43. Su F, Hilton JF, Nardo L, et al. Cartilage morphology and T1rho and T2 quantification in ACL-reconstructed knees: a 2-year follow-up. *Osteoarthritis Cartilage*. 2013;21(8):1058–1067.
44. Alcaraz MJ, Megias J, Garcia-Arnandis I, Clerigues V, Guillen MI. New molecular targets for the treatment of osteoarthritis. *Biochem Pharmacol*. 2010;80(1):13–21.